Mendeleev Communications

Mendeleev Commun., 2025, **35**, 337–340

Polyphenylenepyridines and nitrogen-containing carbon materials based on them

Alexey I. Kovalev,*[a] Alexander V. Naumkin,[a] Maria A. Kovaleva,[a] Sergey S. Bukalov,[a] Suria A. Babich,[a] Natalia S. Revizorova,[a] Sergey E. Lyubimov,[a] Irina A. Khotina[a] and Yaroslav O. Mezhuev[a,b]

[a] *A. N. Nesmeyanov Institute of Organoelement Compounds, Russian Academy of Sciences, 119334 Moscow, Russian Federation. E-mail: kovalev@ineos.ac.ru*

[b] *D. I. Mendeleev University of Chemical Technology of Russia, 125047 Moscow, Russian Federation*

DOI: 10.71267/mencom.7659

On the basis of *p*-diacetylbenzene and 4,4′-diacetylbiphenyl, polyphenylenepyridines with a ratio of pyridine to phenylene rings of 1 : 5–6.5 were synthesized. Their heating in argon at 450, 800 and 1000 °C afforded porous polymers with a specific surface area up to 1146 $m^2 g^{-1}$. X-ray photoelectron spectroscopy of these substances showed that nitrogen atoms in them exist mainly in the form of graphite- and pyridine-like systems.

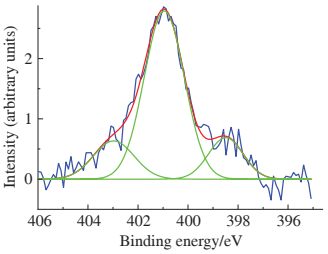

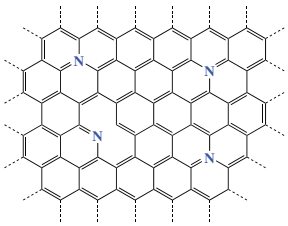

Keywords: polyphenylenepyridines, *p*-diacetylbenzene, 4,4′-diacetylbiphenyl, pyrolysis, pyropolymers, porosity, specific surface area, X-ray photoelectron spectroscopy.

Climate warming and environmental pollution due to the huge consumption of fossil fuels requires the development of new energy technologies.[1,2] The fuel cell is considered as an ideal energy supply system due to its high efficiency of energy conversion, environmental friendliness and the possibility of large-scale application.[3] The cathodic oxygen reduction is one of the critical factors for fuel cells limited by the activation energy barrier and slow kinetics,[4] which significantly limits the commercial application of fuel cells. Platinum is considered the best catalyst for the oxygen reduction since it is characterized by high energy density,[5] but suffers from high cost and poor stability.[6] The use of carbon-based catalysts has attracted much attention and is considered one of the most promising substitutes for Pt-based catalysts.[5,7] Unfortunately, the electrochemical activity of pure carbon materials is low.[8] The introduction of various heteroatoms, such as N, P and Fe, into the carbon framework has proven to be an effective way to increase catalytic activity.[9,10] In particular, nitrogen-containing carbon materials have attracted the most widespread attention.[11,12] Compared to the carbon atom, nitrogen with higher electronegativity can induce partially positive charges on neighboring carbon atoms, which increases the adsorption of oxygen and thereby improves the reaction kinetics.[5,13] In this regard, it is relevant to develop accessible porous nitrogen-containing carbon materials that can be comparable in activity or even better than a platinum catalyst in the oxygen reduction.

Generally nitrogen-containing polymers of linear or hyper-cross-linked type to be subjected to pyrolysis were tested as precursors for electrode materials.[14,15] The most promising precursors for electrode materials were polymers consisting of π-conjugated systems with covalently linked aromatic rings.[16] Carbon materials based on such polymers have nanoporous structures, large surface areas and high chemical stability. Relative nitrogen-containing polymers were produced mainly by metal-complex catalysis procedures which required ultrapure conditions and the use of expensive catalysts.[17–21] Similar disadvantages are inherent in the azide–alkyne cyclization reaction.[22] In this work, conjugated nitrogen-containing polymers were synthesized using a simpler and more technological method.

Previously, we synthesized microporous polyphenylenes by trimerization polycyclocondensation of di- or triacetylarenes in the presence of an triethyl orthoformate and an acid catalyst.[23–27] However, the model reaction between acetophenone and excess triethyl orthoformate in the presence of a non-polar solvent and an acid catalyst produced substances having target phentriyl units along with disubstituted pyrylium salts.[28] After treatment with ammonia, the latter were converted into disubstituted pyridines. This phenomenon herein was put on the basis for the synthesis of polyphenylene pyridines (Scheme 1) when *p*-diacetylbenzene **1a** and 4,4′-diacetylbiphenyl **1b** were used as monomers. The synthesized polymers **2a**,**b** were insoluble in organic solvents. Their IR spectra contain absorption bands at 803 and 1562 cm^{-1}, related to the C–H bending vibrations and the C=N and C=C stretching vibrations of the pyridine ring, respectively.[29]

To obtain porous nitrogen-containing carbon materials, the synthesized polymers were heated in argon at 450, 800 and 1000 °C. For N_2 isotherms of polymer samples **2a-450** and **2b-450** heated at 450 °C, the presence of a hysteresis loop was revealed, which is characteristic of bodies with a slit-like hole or consisting of plane-parallel particles (see Online Supplementary Materials, Figure S2). Based on the obtained adsorption isotherms of samples **2a-450** and **2b-450**, we can conclude that the isotherms belong to type IV adsorption isotherms according to the Brunauer, Deming, Deming and Teller (BDDT)

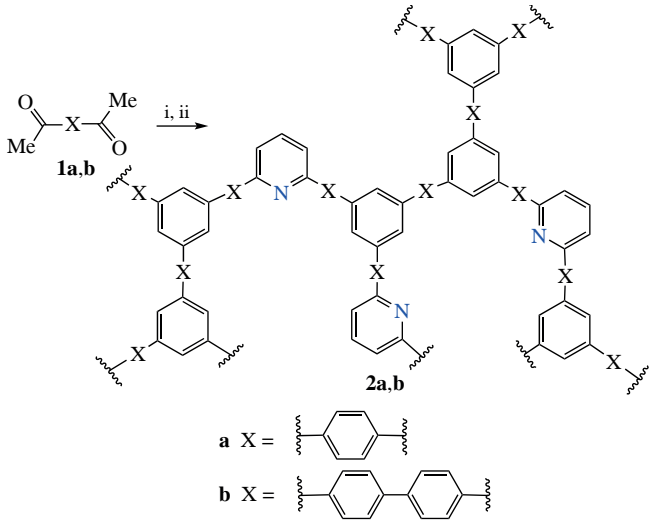

Scheme 1 *Reagents and conditions*: i, $CH(OEt)_3$ (excess), HCl (gas), PhMe, room temperature; ii, NH_3 in $CHCl_3$, room temperature, 65 h.

classification, which is characteristic of mesoporous bodies. Figure 1 shows the adsorption–desorption isotherms of polymer samples **2a** and **2b** heated at 800 and 1000 °C. Based on the obtained isotherms, we can conclude that the isotherms belong to type I adsorption isotherms, which is characteristic of microporous bodies.

Table 1 shows the characteristics of the heat-treated polymer samples. In polymer samples heat-treated at 450 °C, the amount of nitrogen in terms of the ratio of pyridine and phenylene rings is 1 : 5–6.5. With an increase in the heating temperature, the specific surface area of the samples according to BET increases sharply. At the same time, the value of the specific surface of the polymer samples heated at 450 and 800 °C is not affected by the influence of the structure of the initial monomer unit. However, for the polymer samples obtained at 1000 °C, this influence is already noticeable. Thus, the S_{BET} value for the polymer sample

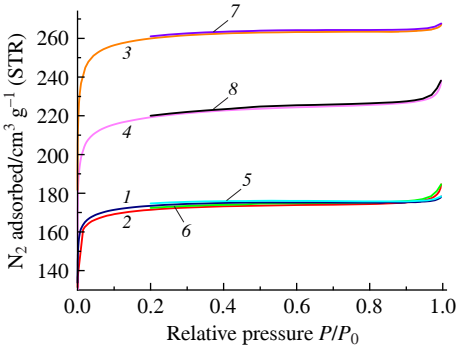

Figure 1 N_2 adsorption isotherm for samples (*1*, navy) **2a-800**, (*2*, red) **2b-800**, (*3*, orange) **2a-1000**, and (*4*, magenta) **2b-1000**, as well as N_2 desorption isotherm for samples (*5*, cyan) **2a-800**, (*6*, green) **2b-800**, (*7*, violet) **2a-1000**, and (*8*, black) **2b-1000**.

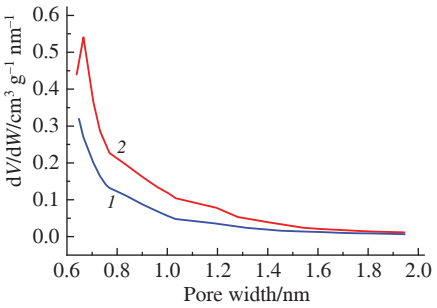

Figure 2 HK pore size distribution for samples (*1*, blue) **2a-800** and (*2*, red) **2a-1000**.

based on *p*-diacetylbenzene **2a-1000** is 1146 $m^2\ g^{-1}$, while for the polymer sample based on 4,4′-diacetylbiphenyl **2b-1000** it is 970 $m^2\ g^{-1}$. It should be noted that for the samples heated at 800 and 1000 °C, the proportion of micropores is 0.96–0.97. At the same time, the influence of the structure of the initial monomer unit of the polymer on the volume of micropores in the heat-treated polymer samples is similar to the influence exerted on the specific surface area of the polymers.

Figure 2 show differential curves of the distribution of micropores by size according to the Horvath–Kawazoe method. The main fraction of micropores for samples obtained at 800 and 1000 °C has pores of 0.6–0.7 nm in size (see also Figure S3). Thus, the structural rearrangement of polymer samples during the transition from 800 to 1000 °C has little effect on the pore size of the samples.

It was previously noted that the active sites of the oxygen reduction reaction in nitrogen-containing carbon materials were mainly created by pyridine- and graphite-like nitrogen-containing systems,[30,31] which increased the adsorption of oxygen molecules on neighboring carbon atoms and thus improved the dynamics of the oxygen reduction reaction.[32]

In order to establish the type of nitrogen-containing system in the heat-treated polymer samples, the latter were studied using X-ray photoelectron spectroscopy. In the high-resolution spectra of the polymer samples heated at 450 °C (**2b-450**), 800 °C (**2b-800**) and 1000 °C (**2b-1000**), only peaks corresponding to

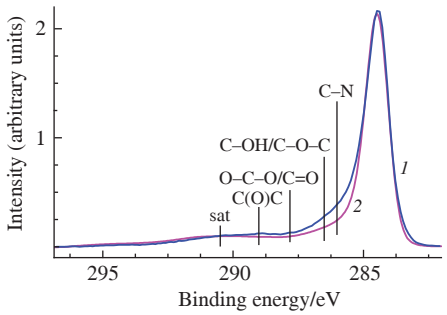

Figure 3 C 1s XPS spectra of samples (*1*, blue) **2b-1000** and (*2*, magenta) HOPG.

Table 1 Characteristics of heat-treated polymers.

Sample	Elemental composition (%)			S_{BET}/$m^2\ g^{-1}$	S_{micro}[a]/$m^2\ g^{-1}$	S_{micro}/S_{BET} (%)	V_{micro}[b]×10^3/$cm^3\ g^{-1}$
	C	H	N				
2a-450	88.72	4.94	2.70	13.9	7.9	56.27	3.33
2a-800	91.13	1.38	1.41	764	747	97.74	261
2a-1000	92.96	1.05	0.49	1146	1117	97.39	389
2b-450	90.14	5.17	2.22	9.9	7.1	71.76	2.95
2b-800	92.20	1.19	1.41	756	735	97.28	256
2b-1000	92.20	1.07	0.78	970	930	95.85	322

[a] Specific surface area of micropores. [b] Specific volume of the micropores according to the t-method.

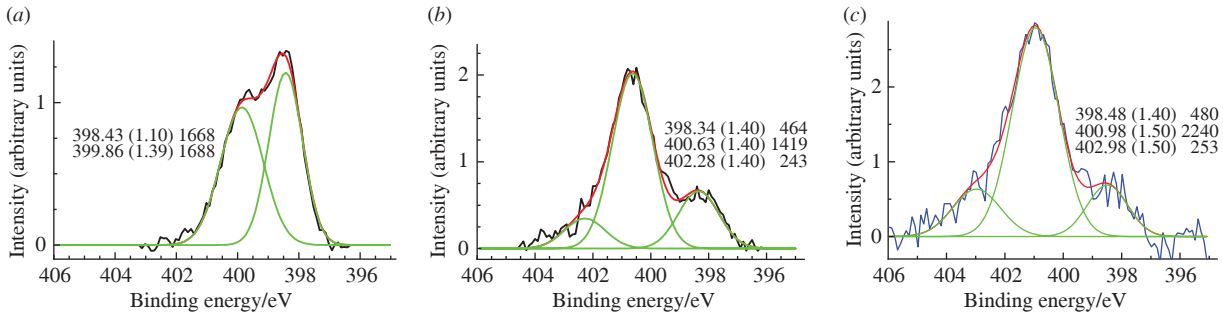

Figure 4 N 1s XPS spectra of (*a*) sample **2b-450**, (*b*) sample **2b-800** and (*c*) sample **2b-1000**.

the elements included in the samples were detected (Figure 3). It should be noted that the elemental composition obtained by XP spectroscopy and elemental analysis differs significantly. In particular, the amount of nitrogen determined by elemental analysis is almost 2 times higher than that determined by XP spectroscopy (see also Figure S4). This discrepancy is probably due to volumetric and surface measurements, respectively.

High-resolution C 1s photoelectron spectra of the studied samples are normalized by the intensity of the main peak; vertical lines show the positions characteristic of possible chemical groups. The descriptor of the sp^2-state in the C 1s spectra is a satellite peak at ~290.5 eV, attributed to the π–π* plasmon. In the C 1s spectra of sample **2b-450** and 1,3,5-tris(biphenyl-4-yl)benzene, the coincidence of satellite peaks indicates that the shape of the spectral line is mainly determined by the phenylene rings and the absence of graphite-like carbon (see Figure S4). The difference in signal intensities in the 285.5–287 eV range is due to the presence of nitrogen- and oxygen-containing groups. To assess the graphitization degree after heat treatment in the C 1s photoelectron spectra of samples **2b-800** and **2b-1000**, the spectrum of highly oriented pyrolytic graphite (HOPG) was used (see Figure 3). The HOPG spectrum was fitted into the low-energy region of the spectra by changing its intensity until the best match was achieved, taking into account intensity normalization at ~290.5 eV. The fractions of the graphite-like sp^2-state in the C 1s spectra of samples **2b-800** and **2b-1000** were 0.46 and 0.91 (Figure S5). This indicates that heating at a higher temperature promotes graphitization.

Figure 4 shows the N 1s XPS spectra of the studied samples. The spectrum of sample **2b-450** is described by two peaks at 398.4 and 399.9 eV with similar relative intensities, which can be attributed to pyridine-like nitrogen and C–NH bonds[33] in pyridinium hydroxide formed due to adsorbed water. In the spectrum of sample **2b-800**, three states at 398.3, 400.6 and 402.3 eV with relative intensities of 0.22, 0.67 and 0.11 were resolved, which are attributed to pyridine- and graphite-like nitrogen and NO_x groups, respectively.[33,34] For sample **2b-1000**, peaks at higher binding energies were observed, *i.e.*, 398.5, 401.0 and 403 eV, which may be due to the partial manifestation of differential charging caused by the appearance of regions with noticeably different electrical conductivity. The relative peak intensities are 0.16, 0.75 and 0.09. The observed increase in the graphitization degree in the C 1s spectrum also manifested itself in the N 1s spectrum. Compared to sample **2b-800**, the proportion of graphite-like nitrogen in sample **2b-1000** increased by 0.08.

The Raman spectra of samples **2a-1000** and **2b-1000** contain D and G bands characteristic of carbon materials in the range of 1326 and 1590 cm^{-1} (Figure S6). Weak, wide bands of the second order are observed in the region of 2500–3200 cm^{-1} spectra. The bands of the observed D and G lines are slightly shifted and significantly widened compared to those of graphite. Their half-widths are ~125 and ~95 cm^{-1}, respectively, and the intensity ratio I_D/I_G is >1. By its position, intensity and half-width of the observed lines, the Raman spectrum is typical for disordered sp^2 carbon structures. The spectra are almost identical, which indicates that there is no significant influence of the primary monomer link on the properties of the pyrolyzed carbon material. The observed Raman spectra are similar in their structure and the ratio of the intensities of the D and G bands to amorphous sp^2 carbon. Thus, during the pyrolysis of polyphenylene pyridine, carbonation occurs with the formation of randomly oriented graphene layers, while a significant proportion of heteroatoms remains.

Thus, the optimal heating temperature for polyphenylene pyridine to obtain a graphite-like structure is 1000 °C. In this case, the total proportion of graphite-like and pyridine-like nitrogen in the sample was 91%, which allows for structure **3**.

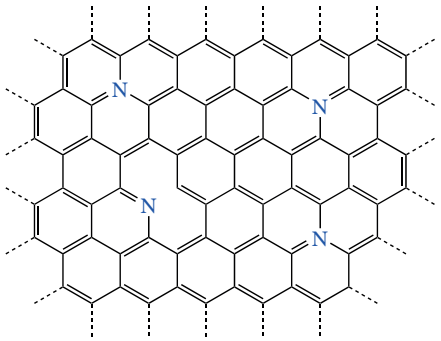

3

Given the well-known fact[31] that the excellent adsorption and reduction of O_2 on N-graphene surfaces is the result of a synergistic effect between pyridine N and graphite N, we have reason to consider pyropolymers based on synthesized polyphenylene pyridines as promising materials for further research in the field of developing components of fuel cell electrodes.

This work was supported by the Russian Science Foundation (grant no. 19-73-20262P).

Online Supplementary Materials

Supplementary data associated with this article can be found in the online version at doi: 10.71267/mencom.7659.

References

1 H. Yu, H. Ma, X. Wu, X. Wang, J. Fan and J. Yu, *Solar RRL*, 2021, **5**, 2000372; https://doi.org/10.1002/solr.202000372.
2 K. Wang, L. Jiang, X. Wu and G. Zhang, *J. Mater. Chem. A*, 2020, **8**, 13241; https://doi.org/10.1039/d0ta01310b.
3 S. Zaman, L. Huang, A. I. Douka, H. Yang, B. You and B. Y. Xia, *Angew. Chem., Int. Ed.*, 2021, **60**, 17832; https://doi.org/10.1002/anie.202016977.
4 X. F. Lu, B. Y. Xia, S.-Q. Zang and X. W. Lou, *Angew. Chem., Int. Ed.*, 2020, **59**, 4634; https://doi.org/10.1002/anie.201910309.
5 L. Dai, Y. Xue, L. Qu, H.-J. Choi and J.-B. Baek, *Chem. Rev.*, 2015, **115**, 4823; https://doi.org/10.1021/cr5003563.

6 J. Liu, M. Jiao, B. Mei, Y. Tong, Y. Li, M. Ruan, P. Song, G. Sun, L. Jiang, Y. Wang, Z. Jiang, L. Gu, Z. Zhou and W. Xu, *Angew. Chem., Int. Ed*., 2019, **58**, 1163; https://doi.org/10.1002/anie.201812423.

7 T. Zhang, F. Cheng, C. Zhao, H. Liu, X. Song, X. Li and W. Luo, *ACS Appl. Mater. Interfaces*, 2021, **13**, 52167; https://doi.org/10.1021/acsami.1c10513.

8 Y. Zhao, J. Wan, H. Yao, L. Zhang, K. Lin, L. Wang, N. Yang, D. Liu, L. Song, J. Zhu, L. Gu, L. Liu, H. Zhao, Y. Li and D. Wang, *Nat. Chem*., 2018, **10**, 924; https://doi.org/10.1038/s41557-018-0100-1.

9 Y. He, D. Gehrig, F. Zhang, C. Lu, C. Zhang, M. Cai, Y. Wang, F. Laquai, X. Zhuang and X. Feng, *Adv. Funct. Mater*., 2016, **26**, 8255; https://doi.org/10.1002/adfm.201603693.

10 X. Wan, X. Liu, Y. Li, R. Yu, L. Zheng, W. Yan, H. Wang, M. Xu and J. Shui, *Nat. Catal*., 2019, **2**, 259; https://doi.org/10.1038/s41929-019-0237-3.

11 Y. Jia, L. Zhang, L. Zhuang, H. Liu, X. Yan, X. Wang, J. Liu, J. Wang, Y. Zheng, Z. Xiao, E. Taran, J. Chen, D. Yang, Z. Zhu, S. Wang, L. Dai and X. Yao, *Nat. Catal*., 2019, **2**, 688; https://doi.org/10.1038/s41929-019-0297-4.

12 L. Lai, J. R. Potts, D. Zhan, L. Wang, C. K. Poh, C. Tang, H. Gong, Z. Shen, J. Lin and R. S. Ruoff, *Energy Environ. Sci*., 2012, **5**, 7936; https://doi.org/10.1039/C2EE21802J.

13 C. Tang and Q. Zhang, *Adv. Mater*., 2017, **29**, 1604103; https://doi.org/10.1002/adma.201604103.

14 J.-S. M. Lee, M. E. Briggs, T. Hasell and A. I. Cooper, *Adv. Mater*., 2016, **28**, 9804; https://doi.org/10.1002/adma.201603051.

15 J. W. F. To, Z. Chen, H. Yao, J. He, K. Kim, H.-H. Chou, L. Pan, J. Wilcox, Y. Cui and Z. Bao, *ACS Cent. Sci*., 2015, **1**, 68; https://doi.org/10.1021/acscentsci.5b00149.

16 F. Xu, D. Wu, R. Fu and B. Wei, *Mater. Today*, 2017, **20**, 629; https://doi.org/10.1016/j.mattod.2017.04.026.

17 H. Sun, P. Zhou, X. Ye, J. Wang, Z. Tian, Z. Zhu, C. Ma, W. Liang and A. Li, *J. Colloid Interface Sci*., 2022, **617**, 11; https://doi.org/10.1016/j.jcis.2022.02.136.

18 N. Meng, H. Li, Y. Liu and Y. Liao, *Electrochim. Acta*, 2022, **402**, 139531; https://doi.org/10.1016/j.electacta.2021.139531.

19 J. A. Mikroyannidis, P. D. Vellis, S.-H. Yang and C.-S. Hsu, *J. Appl. Polym. Sci*., 2010, **115**, 731; https://doi.org/10.1002/app.30958.

20 P. Karastatiris, J. A. Mikroyannidis, I. K. Spiliopoulos, M. Fakis and P. Persephonis, *J. Polym. Sci., Part A*, 2004, **42**, 2214; https://doi.org/10.1002/pola.20050.

21 H. Li, W. Lyu and Y. Liao, *Macromol. Rapid Commun.*, 2019, 1900455; https://doi.org/10.1002/marc.201900455.

22 X. Liu, J. Du, Y. Ye, Y. Liu, S. Wang, X. Meng, X. Song, Z. Liang and W. Yan, *Chin. J. Chem. Eng*., 2022, **42**, 64; https://doi.org/10.1016/j.cjche.2021.09.032.

23 A. I. Kovalev, E. S. Mart'yanova, I. A. Khotina, Z. S. Klemenkova, Z. K. Blinnikova, E. V. Volchkova, T. P. Loginova and I. I. Ponomarev, *Polym. Sci., Ser. B*, 2018, **60**, 675; https://doi.org/10.1134/S156009041805007X.

24 A. I. Kovalev and I. A. Khotina, *Mendeleev Commun.*, 2022, **32**, 244; https://doi.org/10.1016/j.mencom.2022.03.030.

25 A. I. Kovalev, S. A. Babich, M. A. Kovaleva, N. S. Kushakova, Z. S. Klemenkova, Z. K. Blinnikova, A. Yu. Popov and I. A. Khotina, *Polym. Sci., Ser. B*, 2022, **64**, 155; https://doi.org/10.1134/S156009042201002X.

26 I. A. Khotina, O. A. Filippov and A. I. Kovalev, *Mendeleev Commun.*, 2020, **30**, 366; https://doi.org/10.1016/j.mencom.2020.05.035.

27 A. I. Kovalev, A. V. Pastukhov, E. S. Tkachenko, Z. S. Klemenkova, I. R. Kuvshinov and I. A. Khotina, *Polym. Sci., Ser. C*, 2020, **62**, 210; https://doi.org/10.1134/S1811238220020071.

28 M. A. Kovaleva, A. I. Kovalev and I. A. Khotina, *Russ. Chem. Bull*., 2023, **72**, 1186; https://doi.org/10.1007/s11172-023-3888-9.

29 A. I. Kovalev, I. A. Khotina, M. A. Kovaleva, A. V. Naumkin, I. S. Ionova and Ya. O. Mezhuev, *J. Compos. Sci.*, 2023, **7**, 359; https://doi.org/10.3390/jcs7090359.

30 D. Guo, R. Shibuya, C. Akiba, S. Saji, T. Kondo and J. Nakamura, *Science*, 2016, **351**, 361; https://doi.org/10.1126/science.aad0832.

31 P. Yan, J. Liu, S. Yuan, Y. Liu, W. Cen and Y. Chen, *Appl. Surf. Sci*., 2018, **445**, 398; https://doi.org/10.1016/j.apsusc.2018.03.106.

32 H. Deng, Q. Li, J. Liu and F. Wang, *Carbon*, 2017, **112**, 219; https://doi.org/10.1016/j.carbon.2016.11.014.

33 G. Beamson and D. Briggs, *High Resolution XPS of Organic Polymers*, Wiley, Chichester, 1992; https://doi.org/10.1002/sia.740200310.

34 Y. Shao, S. Zhang, M. H. Engelhard, G. Li, G. Shao, Y. Wang, J. Liu, I. A. Aksay and Y Lin, *J. Mater. Chem*., 2010, **20**, 7491; https://doi.org/10.1039/C0JM00782J.

Received: 18th October 2024; Com. 24/7659